Article Identifier
DOI: 10.22032/dbt.58743
URN: urn:nbn:de:gbv:ilm1-2023isc-101:2

60th ILMENAU SCIENTIFIC COLLOQUIUM
Technische Universität Ilmenau, 4 – 8 September 2023
URN: urn:nbn:de:gbv:ilm1-2023isc:1

Preliminary Characterization of Anelastic Effects in the Flexure Mechanism for a new Kibble Balance at NIST

Lorenz Keck[1, 2], Frank Seifert[1], David Newell[1], René Theska[2], Darine Haddad[1]

[1]National Institute of Standards and Technology, Gaithersburg, MD, USA
[2]Technische Universität Ilmenau, Ilmenau, Germany

ABSTRACT

A new Kibble balance is being built at the National Institute of Standards and Technology (NIST). For the first time in one of the highly accurate versions of this type of balance, a single flexure mechanism is used for both modes of operation: the weighing mode and the velocity mode. The mechanism is at the core of the new balance design as it represents a paradigm shift for NIST away from using knife edge-based balance mechanisms, which exhibit hysteresis in the measurement procedure of the weighing mode. Mechanical hysteresis may be a limiting factor in the performance of highly accurate Kibble balances approaching single digit nanonewton repeatability on a nominal $100\,\mathrm{g}$ mass, as targeted in this work. Flexure-based mechanisms are known to have very good static hysteresis when used as a null detector. However, for larger and especially longer lasting deformations, flexures are known to exhibit anelastic drift. We seek to characterize, and ideally compensate for, this anelastic behavior after deflections during the velocity mode to enable a 10^{-8} accurate Kibble balance-measurement on a nominal $100\,\mathrm{g}$ mass artifact with a single flexure-based balance mechanism.

Index Terms – Flexure mechanism, Weighing mechanism, Guiding mechanism, Kibble balance, Anelasticity

1. INTRODUCTION

The Kibble balance principle [1] is one of the methods for the primary realization of the kilogram within the International System of Units (Système international d'unités – SI). It traces the unit of mass back to an unchanging constant of nature, the Planck's constant, and, therefore, establishes a link between macroscopic mass and quantum mechanics [2, 3]. The operating principle, as shown in Figure 1, takes advantage of the fact that an electromagnetic actuator can reversely be used as a generator, which is why the balance uses two operational modes. In one mode, the weighing mode, the actual weighing is performed: a test mass is placed on and off a mass pan attached to an electromagnetic actuator and the current in the coil is adjusted so that the mass pan stays at a defined null position. This is how a force equilibrium between electromagnetic force and weight force of the test mass is established. In the velocity mode, the coil is moved vertically up and down in the magnetic field of a magnetic circuit whereby a voltage is induced depending on the movement velocity following Faraday's induction law. A full mass measurement cycle is usually done by alternating the two modes over several hours to monitor systematic errors and drift. By comparing virtual mechanical with virtual electrical power from a combination of the two operational modes,

the Kibble balance conveniently yields a direct mass/force measurement without a need for external calibration using a reference object [1].

Regarding the design, over the past decades, some choices showed superior performance over others for application in highest accuracy Kibble balances. For the electromagnet, one design can be concluded to be favored over others: as literature often refers to as the Bureau International des Poids et Mesures (BIPM) magnet design [4]. It has a cylindrical precision airgap where a cylindrical coil can move up and down. The magnetic flux is generated by two disc-shaped permanent magnets in repulsion on the upper and lower end of an inner iron yoke creating a radial B-field in the airgap. The magnet has an outer yoke which guides the magnetic flux and encloses the magnetic energy within its footprint. Both the inner and outer yokes are made from soft iron. Besides the magnet, a sub-system that is prominently used for position and velocity measurements in all high-performance balances is a laser interferometric displacement sensor [1].

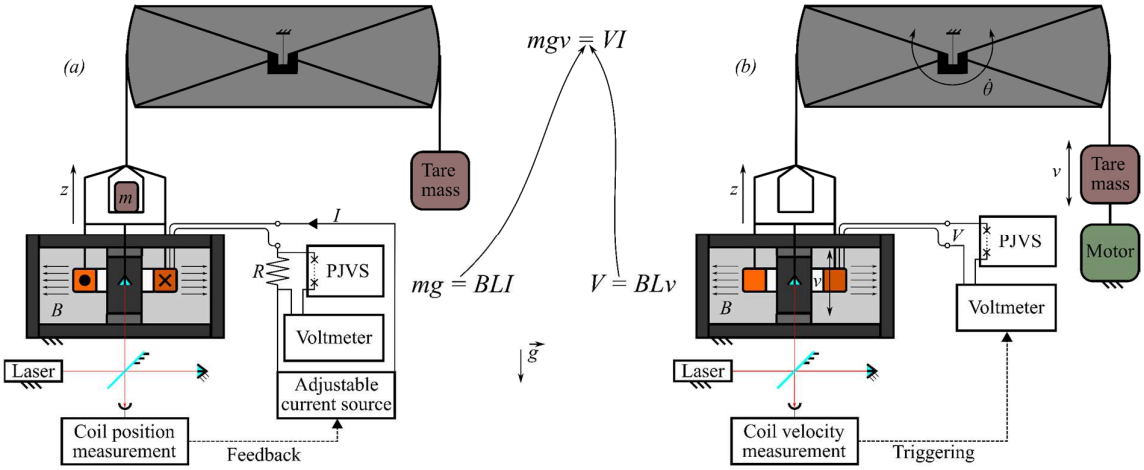

Figure 1: Operating principle of the Kibble balance in the weighing mode (a) and the velocity mode (b). Displayed is a magnetic circuit (permanent magnets – light grey, soft iron yoke – dark grey) with magnetic field B and a test mass m. Weighing mode: The coil is suspended by a mechanism, here displayed as a truncated wheel able to pivot about a flexure. A tare mass for balancing is shown in (b). The electric current I in the weighing mode is adjusted to keep the mass m in static equilibrium. An interferometer can be used as an input for closed loop position control. Electric current is measured using a voltage drop over a known resistor R and compared to the output of a programmable Josephson voltage standard (PJVS) in parallel. The error in this voltage comparison is monitored with a calibrated voltmeter. Velocity mode: An auxiliary electromagnetic actuator (motor) moves the mechanism and thus the coil up and down and a voltage V is induced.

The mechanical part, referring to the suspension of the coil, guiding, and balancing subsystems, however, is very different among most balance designs. Some balances are equipped with two mechanisms, one of which is dedicated for the guiding/moving functionality in the velocity mode, and another one that serves as a balancing/weighing mechanism for the weighing mode. Using two mechanisms for both individual modes of operation allow to optimize each mechanism for its dedicated functionality. This is a convenient starting point for the designer as high precision moving and weighing mechanisms are very delicate instruments which need to be built with great attention to detail to realize the desired functionality precisely. Unfortunately, it faces the challenge of integrating both in one seamlessly working instrument and leaves the experimenter with numerous sub-components which all need to work independently and in combination. For example, a weighing cell suspended from a guiding mechanism – or vice versa – needs to be locked in some way (mechanically, electrically, …) during the velocity mode, to not induce parasitic disturbance to the coil from inertial forces during acceleration of the coil. This is a difficult task under

high vacuum conditions and with the requirement to apply a locking in only one degree of freedom with the necessary stiffness for a 10^{-8} accurate measurement without over-constraining the system. Furthermore, the Kibble balance principle relies on the assumption, that its working conditions do not change between the two modes of operation, because a calibrated magnetic profile from the velocity mode is used as an input parameter for the weighing mode. Complex characterization and corrections for errors are thus necessary to get an accurate measurement. A balance with both modes of operation integrated in one mechanical system with a constrained motion in one defined axis is thus favored from the theorist's and experimenter's point of view. The same virtual displacements are seen by the coil in the weighing mode, as in the velocity mode, which allows cancellation of some of the systematic errors between the two modes [5]. We briefly show the design of the new balance mechanism at NIST before focusing on experimental results for anelastic effects in the flexures of the new Kibble balance.

2. DESIGN OF THE NEW BALANCE MECHANICS

2.1 State of the art

At NIST, knife edge mechanisms have been used for the past decades in four versions of the Kibble balance [3, 6–8]. Each balance had both velocity mode and weighing mode integrated in one mechanical system based the design of a balance wheel rigidly connected to a knife edge which can rotate on a flat. The wheel suspends multifilament bands on both sides. These roll on and off its cylindrical surface and suspend the main coil for the actual mass measurement, a mass pan, and on the other side an auxiliary coil from a smaller electromagnetic actuator to drive the balance in the velocity mode. One of the disadvantages of using a band rolling on a wheel is the fact that a parasitic rotation around the vertical axis of the coil can be induced by stress gradients in the bands, material impurities, or poor alignment of the bands or wheel. This parasitic rotation is usually compensated by an active control element consisting of three capacitors at the coil suspension mounted with $120°$ spacing concentric with the coil so that the capacitors produce an active, electrostatically induced vertical moment to prohibit rotation. Careful alignment is required to make sure to generate a pure vertical rotation in the context of the overall system.

Other Kibble balance groups use a beam balance mechanism instead of a wheel, where this rotation is not present [9, 10]. The advantage of the wheel balance over a beam balance, however, is the fact that the output motion of the suspended parts moves in a linear fashion up and down as the wheel is rotated, whereas a beam balance induces a systematic arcuate movement. The latter might not show up as an error term in the actual mass measurement, if the experimenter uses a beam for both modes of operation [10, 11], but the arc movement gives an inconvenient constraint to the travel range of the coil in the magnetic airgap and, thus, the width of the airgap. One of the Kibble balances using a beam balance as the moving and weighing mechanism is at the National Research Council (NRC) of Canada which has a beam with total arm length 1.2 m to minimize this unwanted lateral displacement.

Another feature that NIST Kibble balances always favored were knife edge pivots (like the NRC beam balance) for constraining the rotation of the wheel [3, 6–8]. Knife edge pivots offer the great advantage of high admissible loads and large excursions, which is exactly what a Kibble balance mechanism requires if the experimenter seeks to execute both modes of operation in one mechanism. Knife edge-based mechanisms have worked well for balances designed and operated during the redefinition of the kilogram until 2018, where balances for 1 kg nominal masses were built. The challenge in a knife edge pivoting on a flat is to optimize the Hertzian contact that can lead to plastic deformation. This leads, even after a small excursion, e.g., during a mass transfer, to hysteretic offsets and, as a result, limits the

repeatability of mass determinations. This is a large uncertainty contribution in existing Kibble balances [12, 13] and especially relevant when measuring lower masses. Hence, a new mechanism was designed with the idea to replace the knife edge-based wheel mechanism. One of the design constraints comes with the goal of compactness in the new Kibble balance. Thus, the footprint of the mechanics should be limited to < 0.5 m in the largest dimension.

2.2 New balance mechanism design

In an effort to move to more compact Kibble balances for lower masses without compromising relative measurement uncertainty, a new balance is under construction at NIST. The nominal target value for mass is 100 g, which should be measured with a relative measurement uncertainty of $< 2 \times 10^{-8}$. This is about what the best balances achieve on nominal 1 kg mass standards [1]. The mass range that will be covered is from 10 g to 200 g. The main objective for the redesign is to reduce uncertainty due to hysteresis from the knife edge in the weighing mode. Thus, a flexure mechanism that was specifically designed for operation in the new Kibble balance as replacement of the knife edge and the rotation control of the coil is under experimental investigation.

As the new mechanism is desired to integrate both functionalities of moving and weighing in one mechanism, a study on flexure geometries well suited for the central pivot (or main flexure) has been conducted [14]. Both finite element analysis (FEA) and analytical equations based on the nonlinear theory of large deflections for bending were used for parametric studies. The main flexure was of particular interest because it suspends the entire balance load and deflects just as any other pivot in the mechanism. A geometry with elliptical shape was found to optimize the stress on the main flexure in the fully deflected state while keeping elastic stiffness low [14]. The analytical equations stem from a partial differential equation system and yield for a simple flexure which is fixed supported on one end with an applied rotation on the other end, see Figure 2:

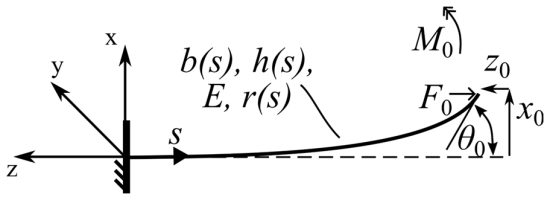

Figure 2: Example for a flexure in deflected state with a moment and force acting on its free end. Parameters: s – variable along neutral flexure axis in deformed state, w – width, h – height, θ – angle, x – displacement of the flexure axis in x, z – displacement of the flexure axis in z, r – curvature of the flexure, E – elastic modulus. The subscript "0" indicates boundary conditions on the free end.

$$\frac{\mathrm{d}M(s)}{\mathrm{d}s} + F\cos(\theta(s)) = 0 \qquad \text{Eq. 2-1}$$

$$\frac{\mathrm{d}\theta(s)}{\mathrm{d}s} - r(s) = 0, \text{ with } r(s) = \frac{M(s)}{EI_z(s)}, \text{ and } I_z = \frac{b(s)h(s)^3}{12} \qquad \text{Eq. 2-2}$$

$$\frac{\mathrm{d}z(s)}{\mathrm{d}s} - \cos(\theta(s)) + 1 = 0 \qquad \text{Eq. 2-3}$$

$$\frac{\mathrm{d}x(s)}{\mathrm{d}s} - \sin(\theta(s)) = 0. \qquad \text{Eq. 2-4}$$

Note that Equations 2-1 – 2-4 can be used to model any flexure in the new mechanism. Here, s defines the neutral flexure axis, M is the moment acting on the flexure, r the curvature, θ the angle of the neutral axis with respect to zero deformation, E the elastic modulus, I_z the moment of inertia due to bending, and x, y the deformation of the flexure along its axis.

The new balance kinematics [15] is based on two sub-mechanisms as shown in Figure 3. One is to ensure the tare functionality in weighing mode – a truncated wheel is used here –

and the other one is to realize a dedicated guiding feature – a folded parallelogram linkage is used to provide an in principle linear motion.

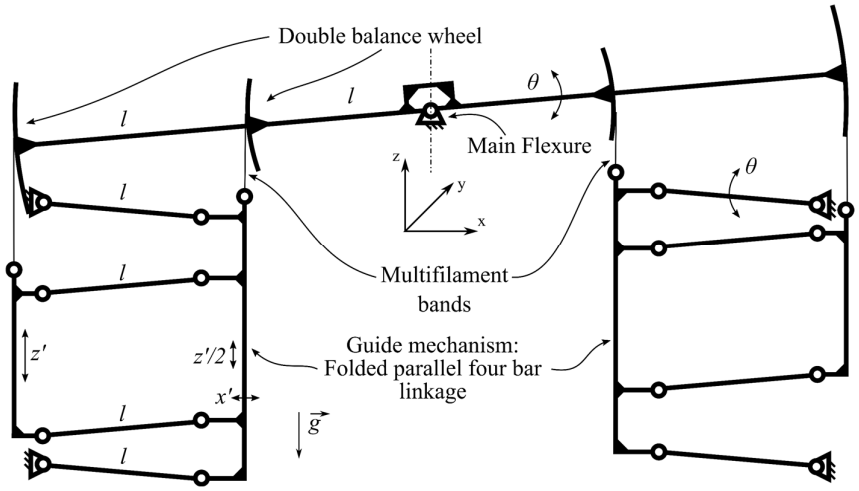

Figure 3: Kinematic chain of the new Kibble balance mechanism – the pivots/flexures are shown with circles. It features a main flexure which connects all the hanging balance components with the frame, a double balance wheel, where the inner wheel has half the diameter ($2l$) of the outer wheel ($4l$), and multifilament bands (indicated as thin vertical lines) connecting the wheel and a guiding mechanism. The guiding mechanism is comprised of a folded parallelogram linkage where both the intermediate (moving by $z'/2$) and final stage (moving by z') are constraint to the inner and outer wheel, respectively. The design is symmetric about the central vertical axis. All flexures contribute to the anelastic after-effect shown in section 4. In the planar case, the kinematic structure is well determined, however, alignments of the sub-components to gravity and with respect to each other are necessary to ensure parallelism of rotational axes and a movement in the true vertical direction. Dimensions not to scale.

The connector between the wheel and the guiding mechanism is designed using multifilament bands that roll off the outer wheel surface and attach to the output stages of the parallelogram. To properly constrain a folded parallelogram linkage, a second kinematic connection is necessary for the intermediate stage. A second wheel with half the diameter of the outer wheel was added and a wire instead of multifilament band can be used for that constraining function.

As for the material, metals with low internal damping, i.e., high mechanical quality factor, are favored for the flexures. Usually, in ultra-high-quality oscillators with low frequency, experimenters employ, e.g., sapphire, or fused silica for flexures or torsion fibers [16—21]. However, machining flexures for a Kibble balance mechanism from these materials imposes a severe challenge to feasibility. Another practical constraint is the fact that the mechanism should be able to resist transient loads, and brittle materials like fused silica or sapphire are known to be problematic in this regard. The metal of choice for experimenters in the field of flexures and high-quality oscillators is usually precipitation hardened Copper Beryllium (Cu-Be) alloy [22, 23] due to yield strengths over $1000\,\mathrm{MPa}$, relatively low internal material damping, excellent machinability for thin flexures and high admissible loads in tension and bending. This material is used for the flexures in this work.

3. THEORY OF ANELASTICITY

Flexures made from metal alloys exhibit anelastic relaxation behavior which is in literature often tied to movement of dislocations in the atomic lattice after a change in strain [22–26]. This causes a material damping effect of flexure oscillators in pendulums of higher frequencies $> 10^{-4}$ Hz [25], but also a time dependent relaxation process of the flexure material after a static deflection [22, 25]. The latter is a deviation of the usual assumption of ideal materials that follow Hooke's law, and a necessary addition for modelling materials in high precision flexure applications [22]. In a weighing mechanism, this anelastic behavior shows up as a nonlinear restoring force/torque drift after deflection from a mass exchange or other unwanted disturbance. Hence, accuracy in weighing schemes like ABA (A – mass on, B – mass off, A – mass on) is limited by this nonlinearity. Further nonlinearity can also be induced by poor clamping mechanisms of flexures, where a stress gradient arises near the clamp as the flexure undergoes a change in strain [24]. However, monolithic flexure elements provide a simple way to eliminate this effect. There is no need for the entire mechanism to be monolithic to avoid clamping hysteresis, but the designer needs to ensure that no stress gradient arises where two structural parts connect [24].

3.1 The generalized Maxwell solid

Nonlinear elastic processes in materials can be approximated using the simple Maxwell solid model [27]. It consists of a spring with a spring-dashpot element in parallel with one relaxation process of time constant τ. This model was later found to be inaccurate when compared to measurements of the relaxation from Cu-Be flexures [25]. Thus, the simple Maxwell model is extended to multiple spring-dashpot elements in parallel to a spring to allow for a more complex relaxation process in the material with multiple time constants τ_0 to τ_∞, where each relaxation has the relaxation strength δe independent of frequency [25]. This shall be called generalized Maxwell model. The generalized approach was found to be a much more accurate description of reality when fitted to experimental data on precipitation hardened Cu-Be[1] alloy for both the dynamic oscillation experiment and the static relaxation test [22, 25].

The authors in [25] suggested to extend the ideal material model following Hooke's law and added an imaginary Young's modulus term $\delta E(\omega)$, called modulus defect depending on the angular frequency ω, to the relaxed modulus E_0, i.e.,

$$E(\omega) = E_0 + \delta E(\omega). \qquad \text{Eq. 3-1}$$

Note that a frequency dependent real term for Young's modulus usually exists as well, but it is neglected here due to its irrelevance for damping [25]. An imaginary part of the bending stiffness results from Equation 3-1 as

$$c(\omega) = c(E_0 + \delta E(\omega)). \qquad \text{Eq. 3-2}$$

In case of the Kibble balance, the relaxation effect after deflection is of higher interest than the damping of a free oscillation or even thermal noise. The latter is directly related with internal material damping [28, 29]. This is because the movement during the velocity mode is

[1] The authors in [25] also mention that similar relaxation behavior could be seen in other materials like aluminum alloy flexures, tungsten fibers, and agate knife edges.

performed using closed loop feedback on the velocity or voltage signal, so internal material damping has no relevant negative effect to the velocity. However, after the large excursions of the balance from the velocity mode, a relaxation drift is expected to compromise linearity in the force signal during the weighing mode (both modes alternate multiple times).

In publications thus far, the anelastic after-effect was always calculated based on a flexure of constant geometry as in [22, 25]. Analytical expressions can be found in latter publications for flexures of constant shape in the bending region. For more complex flexure geometries as the main flexure in the new Kibble balance mechanism, no straight forward analytical expression exists due to its non-constant shape along the bending axis. However, δc could be calculated by adding the modulus defect δE to the elastic modulus in the equations for nonlinear deflection (Equations 2-1 – 2-4), or, in principle, by the Taylor approximation shown in Equation 13 in reference [30], $\delta c(\delta E(\omega)) = \frac{\mathrm{d}c}{\mathrm{d}E}\delta E(\omega)$. According to [25] and [30], the following relationship describes influential parameters for $\delta E(\omega)$ for a generalized Maxwell solid such as Cu-Be:

$$\delta E(\omega) = \delta e \int_{\tau_0}^{\tau_\infty} f(\tau)\frac{\omega\tau}{1+\omega^2\tau^2}d\tau, \text{ with } f(\tau) = \frac{1}{ln(\tau_\infty/\tau_0)}\left(\frac{1}{\tau}\right), \qquad \text{Eq. 3-3}$$

where $f(\tau)$ is a density function normalized so that $\int_{\tau_0}^{\tau_\infty} f(\tau)\,\mathrm{d}\tau = 1$.

In [27], an equation for the anelastic relaxation torque of a simple Maxwell solid after static deflection of angle θ_0 for time T is given as

$$\Delta A(t) = \Delta A_0\left(1 - e^{-\frac{T}{\tau}}\right)e^{-\frac{t}{\tau}}. \qquad \text{Eq. 3-4}$$

Now, using $\Delta A_0 = \theta_0\delta c_0$ and $\delta c_0(\delta E)$ depending on Equation 3-3 as in [25] yields for the anelastic relaxation torque $\Delta A(t)$ of a generalized Maxwell solid in the time domain:

$$\Delta A(t) = \Delta A_0\left(E_i\left(\frac{T+t}{\tau_\infty}\right) - E_i\left(\frac{T+t}{\tau_0}\right) - E_i\left(\frac{t}{\tau_\infty}\right) + E_i\left(\frac{t}{\tau_0}\right)\right), \qquad \text{Eq. 3-5}$$

with $E_i(x) = \int_x^\infty \frac{e^{-u}}{u}\mathrm{d}u$.

In [25], a theory was developed, which yielded an expression for the frequency-independent relaxation strength δe based on factors like lattice interplate spacing, the Burgers vector of dislocations and a stress ratio of applied stress to flow stress. Three years thereafter, this was revoked [24], when a systematic analysis of stress-dependence in damping of Cu-Be alloy flexures and torsion strips indicated only a minor effect of the modulus defect on the mean stress. However, in a publication two years after [24], the authors revisited their result again with the same data from [24] and correctly included a gravitational restoring term in their torsion pendulum, which then showed a slightly nonlinear material damping dependence on the mean stress [23].

3.2 Anelasticity in the Kibble balance

Displacements of the balance mechanism in the Kibble balance have two main causes: (1) a mass exchange procedure usually disturbs the balance for a short amount of time < 15 s due to transient impact of the mass on the mass pan. This disturbance is not static and usually the maximum amplitude is $< \pm 20$ µm, which yields $\theta_0 < \pm 0.1$ mrad for the present mechanism.

And (2) the velocity mode requires large excursions where the flexures in the new mechanism need to pivot about $\theta_0 = \pm 7^\circ$ to ensure sufficient travel for precise information about the magnetic profile [15]. This induces large amounts of stress around a mean position/stress in an oscillatory manner and the phase-delay of the anelastic response is expected to yield a characteristic, anelastic drift. This is immediately followed by a weighing cycle, so the anelastic effect from the velocity mode impacting the weighing shall be investigated. Since the excursions in the velocity mode are so much larger than during a mass exchange, the focus in this work is on the relaxation response of the balance mechanism to oscillatory displacements with large amplitudes. Published experimental results on anelastic after-effect in metal flexures were, to the best of the authors' knowledge, made for flexures after static deflection for a certain amount of time [25] and the analytical description in [25] is not sufficient to predict systematics in the anelastic drift from velocity mode excitations. A series of experiments has been started to investigate the nonlinearity from the moving mode in the new Kibble balance mechanism systematically in more detail. First results of this study are presented in the next section.

4. EXPERIMANTAL INVESTIGATIONS

4.1 Test setup

The balance mechanism designed in [15] was machined, assembled, and aligned so that a movement is free of buckling, and the output stages move aligned with the vertical to within better than ± 10 µm for displacements of the final stage of approximately ± 25 mm. The apparatus, see Figure 4, is housed in a vacuum chamber in a laboratory 12 m underground and the vacuum pressure is < 0.001 Pa. Currently, the electromagnetic actuator on the counter mass side is used for feedback operation. The main coil suspension is being machined as of the date of this manuscript and will be assembled and attached to the balance in future work. Dummy masses suspended from gimbals attached to the output stages on either side of the mechanism mimic the suspended load to the balance in real operation later. The total combined load suspended from the main flexure is approximately 15 kg and the balance readout was calibrated to within 0.1 % by using a reference weight.

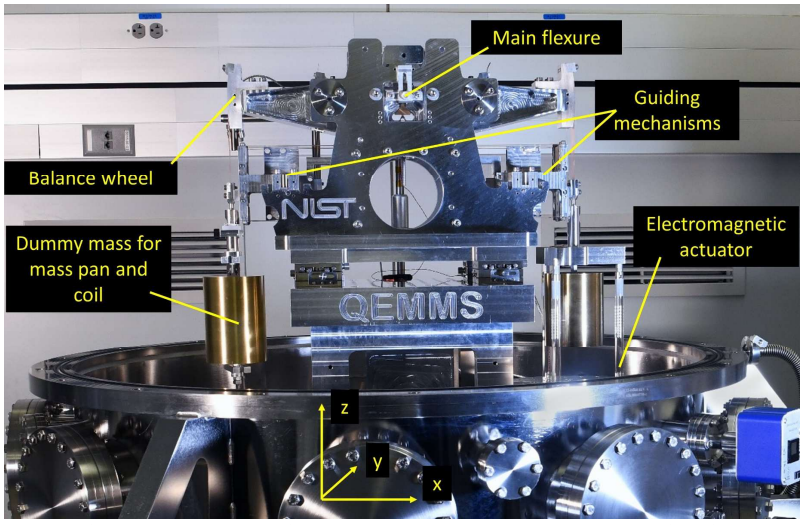

Figure 4: Experimental setup of the new balance mechanism in the vacuum chamber of the future Kibble balance at NIST. The cylinders to the left and right are dummy masses to simulate the weight suspended by the balance later when all components are suspended. The counter mass coil and magnet to the right ("Electromagnetic actuator") are used for feedback operation. An interferometer (not shown) was attached to the output stage for closed loop position feedback of the mechanism displacement.

In contrary to actual weighing with a Kibble balance, where a mass imbalance is generated on the mass pan due to the mass on- and mass off states [1], the apparatus here is used as a null detector, which is a reasonable simplification for the experimental evaluation of the mechanical system. The equilibrium of the mechanism was adjusted so that, after pumping vacuum, the balance reads close to zero force – within ± 500 µN. This reduces magnetic hysteresis, which is easily confused with mechanical hysteresis, and avoids excessive thermal heating of the coil in a non-steady force state, e.g., when moving the balance. The stiffness in the weighing position is well below 0.1 N/m and the coil is electrically in series with a 1 kΩ standard resistor, which is in parallel to an integrating 8.5-digit precision voltmeter. The temperature stability in the laboratory is ± 0.2 K. A slightly modified version of a custom low noise current source board [31] was used. The feedback was implemented using a proportional integral derivative (PID) controller with a low pass filter on the D-term and the control loop was programmed fully in hardware on a field programmable gate array (FPGA), where the control frequency was set to 3 kHz.

4.2 First measurements

At first a measurement with $T = 3$ min and 100 µm displacement ($\theta_0 = 0.4$ mrad) was done, where the nonlinear drift due to anelasticity in the flexures was measured over half an hour after returning from deflection, see Figure 5(a). This provides a general sense of the magnitude of anelasticity in the experiment and provides a value for comparison of the new balance mechanism with existing values in literature. The time for the balance to reach the deflected state and come back to the weighing position was approximately 10 s, respectively and displacements happened with an overshoot to the respective target positions of less than 1 µm. For all measurements, the balance was required to reach a stable state which was defined as having a positional standard deviation of less than 10 nm within better than 2 nm deviation of the balance mean position from its nominal position. Fitting Equation 3-5 to the experimental data showed excellent agreement between the qualitative behavior of the new flexure mechanism and what was reported from literature. Note that it was empirically found that $\tau_0 \approx 10$ s and $\tau_\infty \approx 5000$ s for precipitation hardened Cu-Be alloy [25]. The result for following graphs was translated to a linear force instead of a moment reaction as in [22, 25] or Equation 3-5.

(a) *(b)*

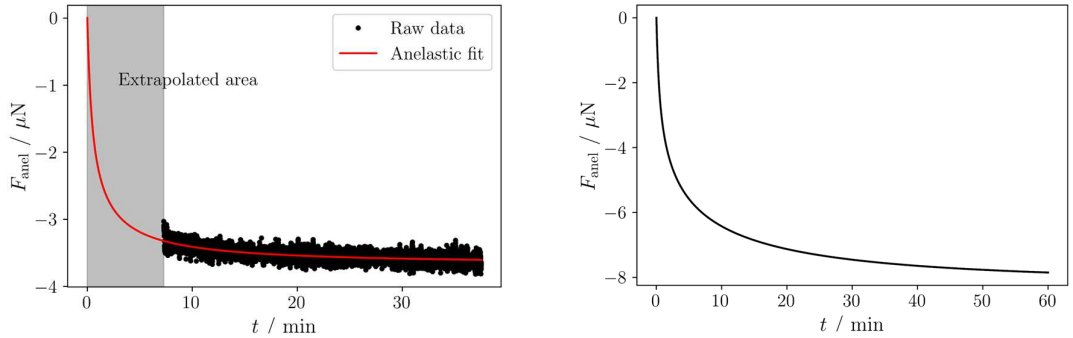

Figure 5: (a) Anelastic drift of the flexure mechanism after 100 µm *displacement of the new flexure mechanism for 3* min. *A major part of relaxation happens during the first five minutes after returning to the zero position. However, the anelastic drift goes on for more than* 30 min *after returning to the nominal zero position. The black dots are raw data, and the red line is the least square fit for anelastic relaxation following Equation 3-5. For explanation on the extrapolation and how the data gathering started, the reader is referred to the text.* (b) *Anelastic drift (from least squares fit) of the flexure mechanism after the simulated velocity mode as described in the text. The anelasticity after the velocity mode is much larger than from small static deflections.*

It takes quite some time for the balance to reach the actual target position with respect to the criterion mentioned above, because the optimized PID gains for a low noise force measurement cannot follow the harsh drift of the anelastic response in the flexures immediately. With the current gain settings, this is about 300 s to 400 s after returning the balance to nominal zero position. This is indicated by the shaded area in Figure 5(a). Accounting for this dead-time in the measurement process and extrapolating the anelastic fit shows that a relaxation of multiple micronewtons results.

From the anelastic fit, a value of $\delta c_0 = 6.7 \times 10^{-4}\,\mathrm{Nm/rad}$ is found, which compares well to published values from previous literature [22]. This result is particularly promising considering the main flexure in the present mechanism had to be stiffer than in [22] and additional guide flexures are used. A total of 25 flexible elements, including the bending of the multifilament bands, are present in the new balance mechanism and contribute to anelasticity.

A second test was performed to investigate the balance response after a velocity mode. The mechanism was slowly exercised in a sinusoidal manner with ± 25 mm displacement in five cycles, which took a total time of about 23 min. After that, the anelastic drift was recorded and the drift-function was fitted. Figure 5(b) shows the results for 1 h measurement time. The nonlinear anelastic drift after the large excursions during the velocity mode has (1) a larger force-drop in the beginning of the relaxation, and (2) the decay happens over a much larger time scale. (2) indicates that the effective time of deflection T seen by the flexures, if one were to substitute the sinusoidal excursions with a constant deflection of time T, is much larger than in the previous experiment. An ABA mass measurement of 100 g mass with a relative nonlinear error of about 2×10^{-9} would not be realistic here, as the time for one ABA cycle usually is on the order of 5 min to 10 min, depending on the speed of a mass exchange, and the required integration time.

A method of compensating for the anelastic after-effect was investigated, where the balance mechanism was subject to a counter-bending after the velocity mode was executed. A substantial reduction of the anelastic drift could be seen and, at larger counter-bending amplitudes, a sign switch of the drift could also be achieved. An example for the reduction of the anelastic drift is shown in Figure 6(a). The amplitude of the velocity mode oscillation was the same as for Figure 5(b), but here, a counter-bending of 3.6 mm with the same frequency as the moving frequency was induced before measuring the drift.

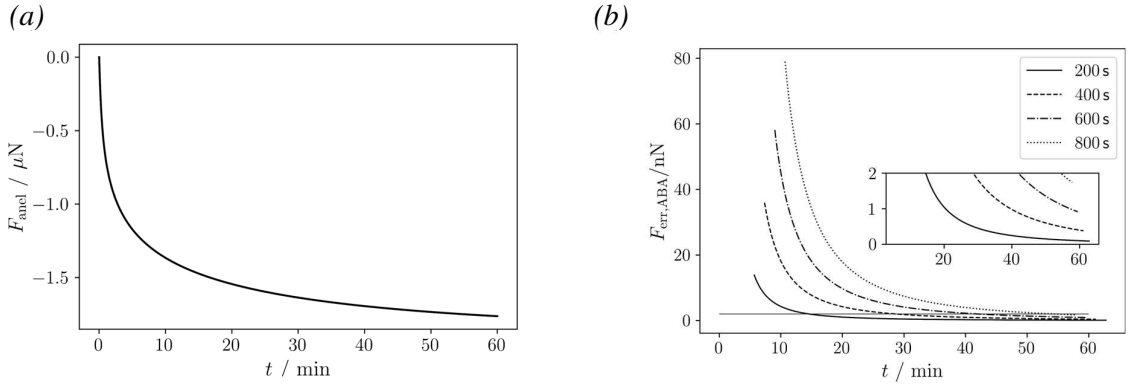

Figure 6: (a) Anelastic after-effect after compensational overshoot of 3.6 mm *after the velocity mode. (b) Worst-case nonlinearity error during ABA-weighing resulting from anelastic drift in (a) for ABA-cycle times of* 200 s, 400 s, 600 s, and 800 s. *The horizontal line in (b) indicates the target nonlinearity error of* 2 nN.

In Figure 6(b), the error induced by anelastic nonlinearity for ABA weighing schemes of different cycle times is shown. Even for an ABA cycle of 200 s the worst-case nonlinearity

error is below the acceptable threshold of 2 nN only after approximately 15 min of measuring.

5. CONCLUSIONS AND FUTURE WORK

A new Kibble balance mechanism was designed at the National Institute of Standards and Technology. This flexure-based design is currently under investigation to study performance during velocity mode and weighing mode with focus on the anelastic behavior of the flexures. The results of the experiments show clear nonlinear anelastic reaction of the flexures in the new mechanism attributed to the large excursions from velocity mode. A reduction of this effect can be realized by counter-bending the mechanism before starting a mass measurement, which can be a powerful tool to mitigate nonlinear material errors and allow for the required accuracy in measurement.

More thorough systematic studies are necessary to show reliability of a compensation of the nonlinear force drift due to anelasticity. Furthermore, the effect of the deflection history to successive velocity modes and weighing modes shall be investigated in future studies, as anelastic effects in flexures are known to be present to frequencies $< 10^{-4}$ Hz [25]. As such, it may be that a relaxation process from a previous velocity mode still has impact on the flexure reaction after the next velocity mode, due to its very low frequency response. This makes characterization of the drift with respect to displacement history highly dependent on the actual parameters of movement (amplitude, motion profile, velocity, …). Future work will investigate compensation algorithms to "reset" or "zero" the flexures in the mechanism after each velocity mode to ensure unentangled considerations of successive measurements and allow for systematic studies in the Kibble balance for measurements with different velocities. Residual effects of anelasticity on successive measurements can lead to misinterpretation of drift in the instrument and substantially increase difficulty of systematic evaluation of the balance behavior.

Finite element analysis can be a helpful tool to both predict and confirm experimental outcomes. By using a nonlinear material model based on viscoelastic material, numerical simulation with commercial FEA software can be performed. Viscoelastic material is often modelled according to the generalized Maxwell model [32, 33], which is used to describe metal anelasticity as well [22, 25]. To do so accurately in FEA, one would need to have precise knowledge of the actual anelastic properties of the material. This is hard to define because the data for that usually results from a measurement. However, using FEA it should still be possible to use approximate values for the modulus defect and describe the systematic of anelasticity in a flexure sufficiently well. We seek to investigate systematics to nonlinear flexure drift after excursions with different amounts of cycles, amplitudes, loads, geometries, and frequencies.

REFERENCES

[1] Robinson, I.A. and Schlamminger, S. The watt or Kibble balance: a technique for implementing the new SI definition of the unit of mass Metrologia 53 A46 (2016).

[2] Haddad, D. *et al*. Bridging classical and quantum mechanics. Metrologia 53 A83 (2016).

[3] Seifert, F.C. *et al*. A macroscopic mass from quantum mechanics in an integrated approach. Commun Phys 5, 321 (2022).

[4] Li, S. and Schlamminger, S. The irony of the magnet system for Kibble balances—a review. Metrologia 59 022001 (2022).

[5] Kibble, B.P. and Robinson, I.A. Principles of a new generation of simplified and

accurate watt balances. Metrologia 51 S132 (2014).
[6] Olsen, P.T. *et al.* A measurement of the NBS electrical watt in SI units. IEEE Transactions on Instrumentation and Measurement 38 2 (1989).
[7] Williams, E.R *et al.* Accurate Measurement of the Planck Constant. Phys. Re. Lett. 81 12 (1998).
[8] Schlamminger, S. *et al.* A summary of the Planck constant measurements using a watt balance with a superconducting solenoid at NIST. Metrologia 52 L5 (2015).
[9] Thomas, M. *et al*. A determination of the Planck constant using the LNE Kibble balance in air. Metrologia 54 468 (2017).
[10] Sanchez, C.A. and Wood, B.M. Alignment of the NRC watt balance: considerations, uncertainties and techniques. Metrologia 51 S42 (2014).
[11] Robinson, I.A. Alignment of the NPL Mark II watt balance. Meas. Sci. Technol. 23 124012 (2012).
[12] Haddad, D. *et al*. Measurement of the Planck constant at the National Institute of Standards and Technology from 2015 to 2017. Metrologia 54 633 (2017).
[13] Schwarz J.P. *et al*. Hysteresis and related error mechanisms in the NIST watt balance experiment. J. Res. Natl Inst. Stand. Technol. 106 627–40 (2001).
[14] Sauer, A. Master Thesis: Numerical analysis on main flexure pivots for Kibble balance mechanisms. Technische Universitaet Ilmenau. (2022).
[15] Keck, L *et al*. Design of an enhanced mechanism for a new Kibble balance directly traceable to the quantum SI. EPJ Techn Instrum 9: 7, (2022).
[16] Braginsky, V.B. *et al*. Laboratory experiments to test relativistic gravity. Phys. Rev. D 15 8 (1977).
[17] Uchiyama, T. *et al.* Mechanical quality factor of a sapphire fiber at cryogenic temperatures. Physics Letters A 273 (2000).
[18] Shaw, E.A. *et al.* Torsion-balance search for ultralow-mass bosonic dark matter. Phys. Rev. D 105 4 (2022).}
[19] Pratt, J.R. *et al*. Verification of an in situ calibrated optomechanical accelerometer for use as a strong ground motion seismic reference. Metrologia 58 055005 (2021).
[20] Gretarsson, A.M. *et al.* Pendulum mode thermal noise in advanced interferometers: a comparison of fused silica fibers and ribbons in the presence of surface loss. Physics Letters A 270 3–4 (2000).
[21] Uchiyama, T. *et al.* Mechanical quality factor of a cryogenic sapphire test mass for gravitational wave detectors. Physics Letters A 261 1–2 (1999).
[22] Quinn, T.J. The Beam Balance as an Instrument for Very Precise Weighing. Measurement Science and Technology, 3(2):141–159, (1992).
[23] Quinn, T.J. *et al*. The restoring torque and damping in wide Cu-Be torsion strips. Phys. Lett. A 228 36–42 (1997).
[24] Quinn, T.J. *et al*. Stress-dependent damping in Cu-Be torsion and flexure suspensions at stresses up to 1.1 GPa. Physics Letters A 197 197-208 (1995).
[25] Quinn, T.J. *et al*. Materials Problems in the Construction of Long-Period Pendulums. Philosophical Magazine A-Physics of Condensed Matter Structure Defects and Mechanical Properties, 65(2):261–276, (1992).
[26] Cagnoli, G. *et al.* On dislocation damping at low frequencies. Philosophical Magazine A 68 5 (1993).
[27] Nowick, A.S. and Berry, B.S. Anelastic Relaxation in Crystalline Solids Chapt 4 p92. Academic Press, New York and London, (1972).
[28] Saulson, P.R. Fundamental limits to the sensitivity of interferometric gravitational wave detectors. Physical Review D, 42:2437, (1990).
[29] Beilby, M.A. *et al.* Photoelastic measurement of anelasticity and its implications for

gravitational wave interferometers. Rev Sci Instrum 69, 2539–2545 (1998).
[30] Speake, C.C. Anelasticity in flexure strips revisited. Metrologia 55 114, (2018).
[31] Haddad, D. *et al.* Low noise programmable current source for the NIST-3 and NIST-4 Watt balance. Conference on Precision Electromagnetic Measurements, (2012).
[32] Renaud, F. *et al.* A new identification method of viscoelastic behavior: Application to the generalized Maxwell model. Mechanical Systems and Signal Processing 25 3 (2011).
[33] Babaei, B. *et al*. Efficient and optimized identification of generalized Maxwell viscoelastic relaxation spectra. Journal of the Mechanical Behavior of Biomedical Materials 55 (2016).

CONTACTS

Lorenz Keck
email: Lorenz.Keck@nist.gov
ORCID: https://orcid.org/0000-0002-2052-1546

Dr. Darine Haddad
email: Darine.ElHaddad@nist.gov
ORCID: https://orcid.org/0000-0002-9716-3310